Assessment of SIRGAS Ionospheric Maps errors based on a numerical simulation

Claudio Brunini, Emilio Camilion, Francisco Azpilicueta
Facultad de Ciencias Astronómicas y Geofísicas
Universidad Nacional de La Plata
and CONICET, Argentina
claudiobrunini@yahoo.com

1. Introduction

As responsible of the International Terrestrial Reference Frame (ITRF) densification in Latin America, SIRGAS (Sistema de Referencia Geocéntrico para las Américas) manages a continuously operational GNSS network with more than 200 receivers. SIRGAS uses this network to compute regional maps of vertical Total Electron Content (TEC)(Fif. 1) that are released to the community through the SIRGAS web page (www.sirgas.org).

As other similar products (e.g.: Global Ionospheric Maps computed by the International GNSS Service), SIRGAS maps are based on a thin layer ionospheric mode in which the whole ionosphere is represented by one spherical layer of infinitesimal thickness at a fixed height and a geometrical mapping function that relates the vertical to the slant TEC.

This contribution aims to characterize the errors associated to the thin layer ionospheric mode. The work relies upon a numerical simulation performed with an empirical model of the Earth's ionosphere, which allows creating a realistic but controlled ionospheric scenario, and then evaluates the errors that are produced when the model is used to reproduce those ionospheric scenarios.

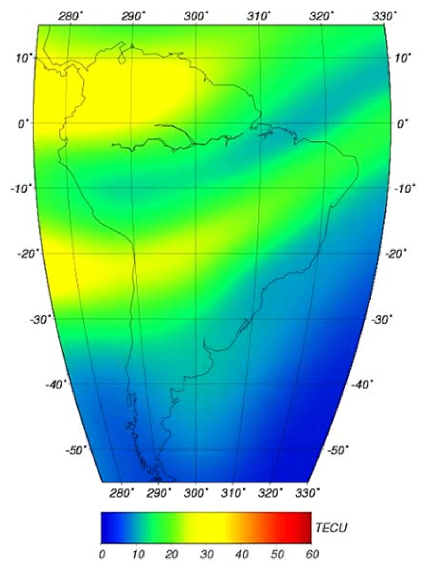

Fig.1. SIRGAS vTEC for day 205, 2005, 0 UT.

2. Thin layer ionospheric model

The whole ionosphere is represented by one spherical layer of infinitesimal thickness at a fixed height, h_L.

The slant TEC ($sTEC$) along a given satellite- to-receiver line-of-sight (LOS) is related to the vertical TEC ($vTEC_L$) at the ionospheric penetration point (IPP) by:

$$sTEC = \sec z_L\left(h_L\right)\cdot vTEC_L, \tag{1}$$

where $z_L(h_L)$ is the LOS z_E zenith angle at the IPP and $\sec z_L\left(h_L\right)=\left[1-\left(r_E\sin z_E\right)^2/\left(r_E+h_L\right)^2\right]^{-1/2}$ (z_E is the zenith angle at the observing point and r_E the Earth's radius) is the geometrical mapping function).

The $vTEC_L$ is parameterized as a function of time, t, and the geographic latitude, φ_L, and longitude, λ_L, of the IPP:

$$vTEC_L = f_L\left(t,\varphi_L,\lambda_L;x_0,\ldots,x_n\right). \tag{2}$$

The parameters, x_i, $i=0,\ldots,n$, and the satellite + receiver inter-frequency biases (IFB), $\beta=\beta_R+\beta_S$, are estimated from the GNSS observations based on the following equation of observation:

$$L_I+v_I=\sec z_L\left(h_L\right)\cdot f_L\left(t,\varphi_L,\lambda_L;x_0,\ldots,x_n\right)+\beta, \tag{3}$$

where L_I is the dual-frequency GNSS ionospheric observable and v_I is the associated observational error.

3. Numerical simulation

The vTEC distribution in the SIRGAS region is characterized by large horizontal gradients caused by the Appleton Anomaly (Fig. 3).

These gradients are particularly noticeable during daytime and particularly in the North-South direction.

In order to study the errors caused by these gradients in the thin layer ionospheric model, the following fictitious scenario is considered (Fig.2):

- 14 LT;
- A GNSS satellite moving along the 300º meridian;
- An array of 7 GNSS receivers along the same meridian, one every 10º of latitude from –40º to 20º;
- LOS zenith angles from every receiver covering all zenith angles, from 0º to ±90º (North and South of the observing point).

Fig. 2. Geometry for the numerical simulation.

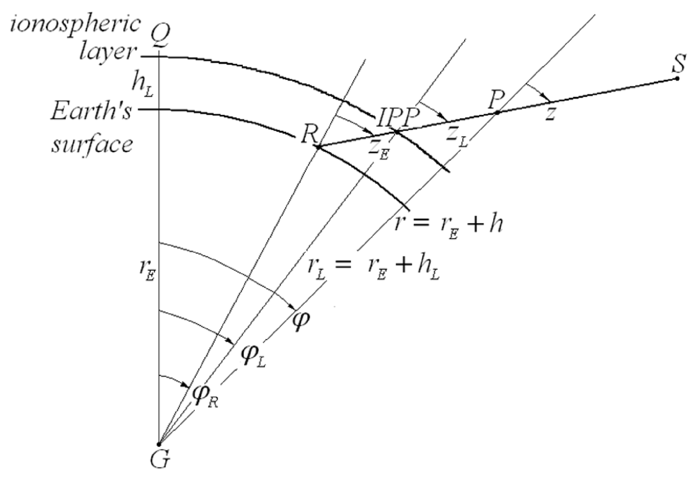

Plane of the figure ≡ 300º meridian;
G ≡ geocentre;
$\overline{GQ}$ ≡ projection of the Equator on the meridian plane;
R ≡ fictitious GNSS receive at geography latitude φ_R;
S ≡ fictitious GNSS satellite on the meridian plane;
$r=r_E+h$, φ ≡ position of a point, P, along the LOS.

The NeQuick electron density model is used to simulate the electron density distribution.

For this particular geometry NeQuick reduces to a two-dimensional function, $N_{eNQ}\left(r,\varphi\right)$, so that:

$$vTEC=\int_{r_E+h_1}^{r_E+h_2}N_{eNQ}\left(r,\varphi_L\right)\cdot dr, \tag{4.a}$$

$$sTEC=\int_{r_E+h_1}^{r_E+h_2}N_{eNQ}\left(r,\varphi\right)\cdot\frac{dr}{\cos z}, \text{ and} \tag{4.b}$$

$$vTEC_L=\cos z_L\left(h_L\right)\cdot sTEC, \tag{4.c}$$

where h_1~100 km and h_2~1000 km are the nominal bounds of the ionosphere.

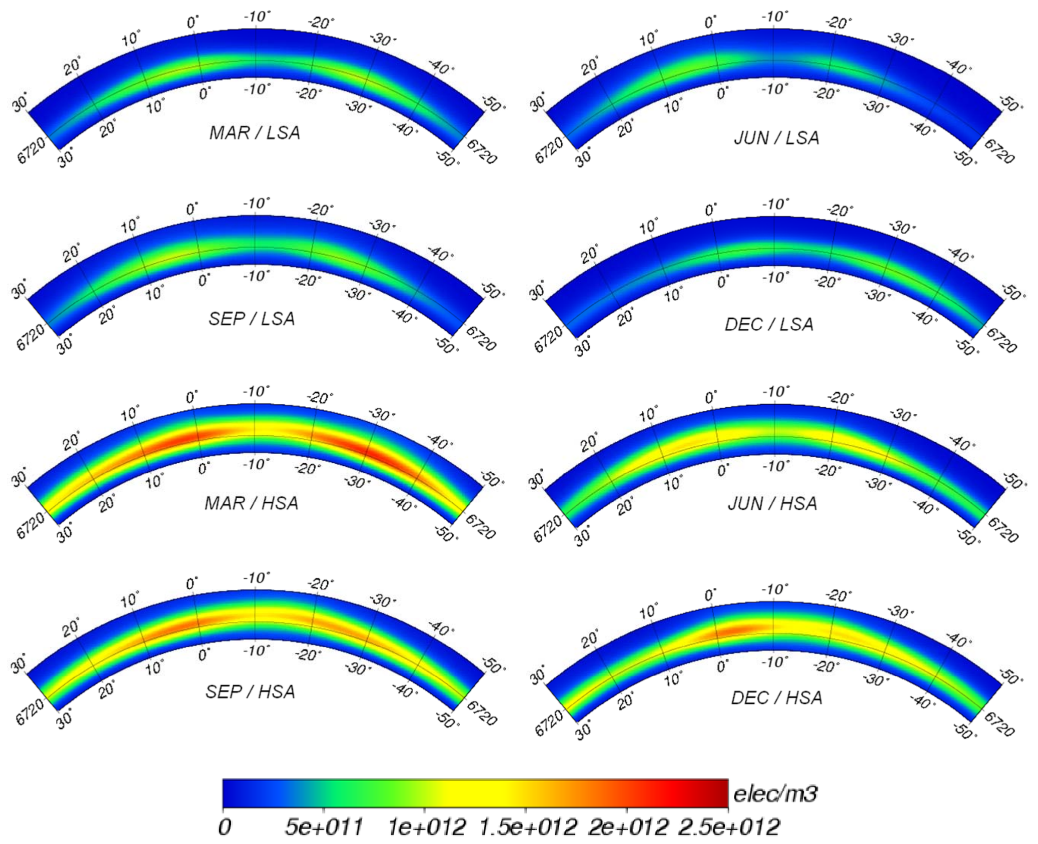

Fig. 3. Latitudinal cuts of the electron density distribution computed with the NeQuick model along the 300º meridian, from 100 to 1000 km of height, at 14 LT, for March (MAR), September (SEP), June (JUN) and December (DEC), and for low (LSA) and high (HSA) solar activity, simulated with the NeQuick electron density model (the solid line at 6720 km represents the ionospheric layer at 350 km).

4. Assessment of the mapping function error

The vTEC error due to the use of the mapping function is:

$$\varepsilon\left(h_L\right)=vTEC_L-vTEC=\cos z_L\left(h_L\right)\cdot\int_{r_E+h_1}^{r_E+h_2}N\left(r,\varphi\right)\frac{dr}{\cos z}-\int_{r_E+h_1}^{r_E+h_2}N\left(r,\varphi_L\right)\cdot dr. \tag{5.a}$$

The systematic component of this error is characterized by the average of all the observed LOS (z_E from 0º to ±90º) from the 7 GNSS receivers:

$$\left\langle\varepsilon\left(h_L\right)\right\rangle=\frac{1}{7}\sum_{\varphi_R}\frac{1}{180^\circ}\int_{z_E=-90^\circ}^{z_E=+90^\circ}\varepsilon\left(h_L\right)\cdot dz_E, \tag{5.b}$$

and the varying component is characterized by the average of the (absolute value) deviations:

$$\delta\varepsilon\left(h_L\right)=\frac{1}{7}\sum_{\varphi_R}\frac{1}{180^\circ}\int_{z_E=-90^\circ}^{z_E=+90^\circ}\left|\varepsilon\left(h_L\right)-\left\langle\varepsilon\left(h_L\right)\right\rangle\right|\cdot dz_E, \tag{5.c}$$

The error assessment is performed for 5 levels of solar activity: low (F10.7 = 70 SFU), intermediate-low (100 SFU), intermediate (130 SFU), intermediate-high (160 SFU), and high (190 SFU); for the 12 months of the year; and for 11 heights of the ionospheric layer, from 350 km to 550 km, with steps of 25 km.

The results of this assessment are summarized in Figs. 4 and 5.

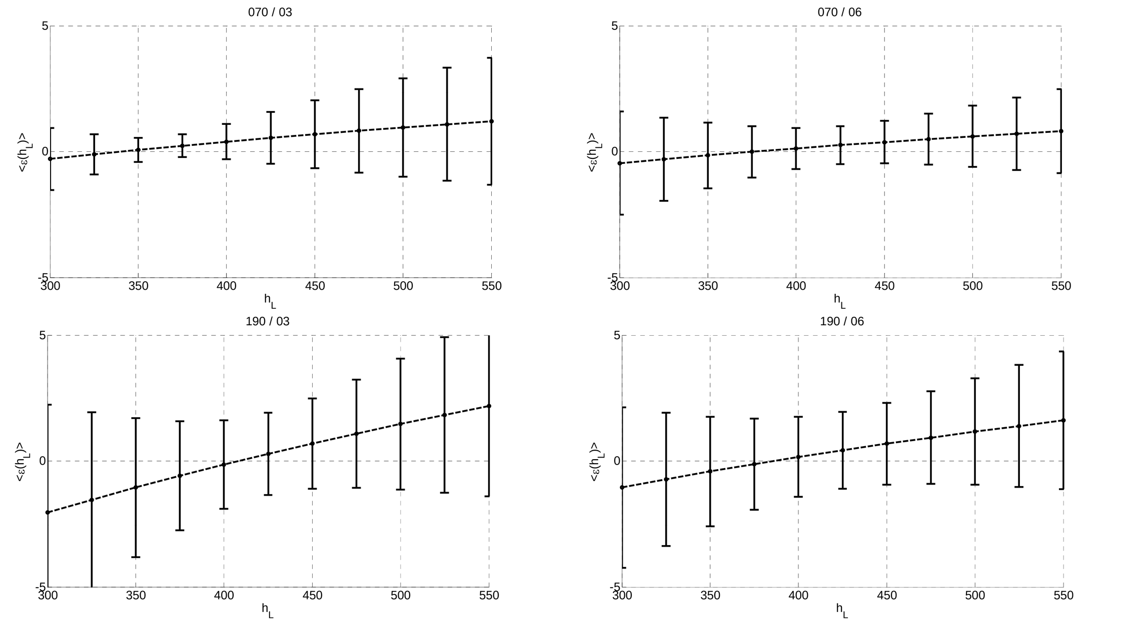

Fig. 4. Variation with the height of the ionospheric layer, h_L (km), of $\left\langle\varepsilon\left(h_L\right)\right\rangle$ (points) and $\delta\varepsilon\left(h_L\right)$ (bars), in TECu, for low (F10.7 = 70 SFu) and high (F10.7 = 190 SFu) solar activity, and for March (03) and June (06).

The systematic effect of the mapping function error, i.e.: $\left\langle\varepsilon\left(h_L\right)\right\rangle$, cancels at an ionospheric layer height $h_{L,0}$ that varies with the solar activity and month.

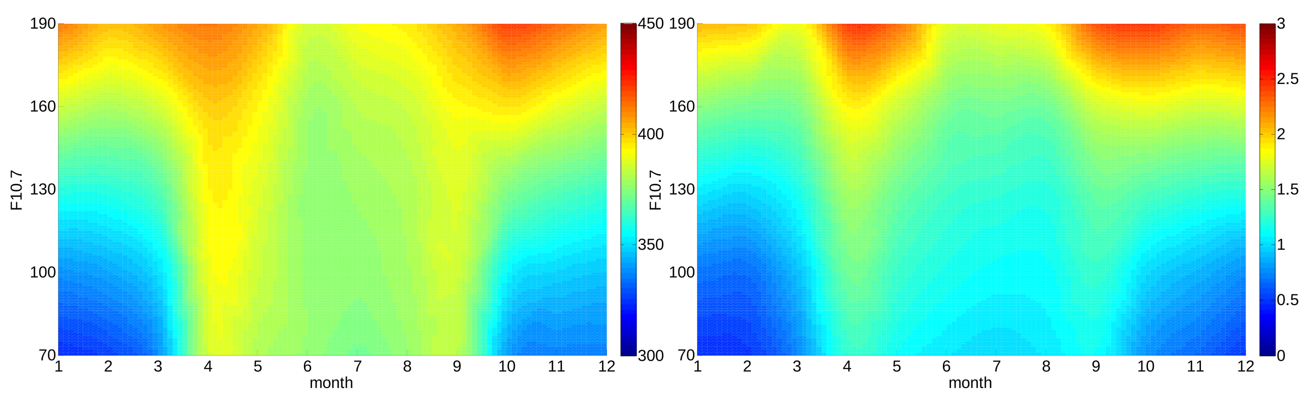

Fig. 5. Variation with the solar activity and month of $h_{L,0}$ (km) (left) and $\delta\varepsilon\left(h_{L,0}\right)$ (TECu) (right).

5. Assessment of the in the vTEC and IFB estimation errors

The $\varepsilon(h_L)$ error discussed in Section 4 propagates to the unknowns of Eq. (3) when their values are estimated from the GNSS observations and causes an incorrect estimation of both, the $x_0,\ldots,x_n$ parameters of the $vTEC_L$ function and the IFB, β.

In order to study the error propagation, a Legendre's functions expansion is used to represent the latitudinal variation of the vTEC along the 300º meridian, from –50º to +30º of geographic latitude, at 14 LT:

$$vTEC=f\left(\varphi;x_0,\ldots,x_n\right)=\sum_{l=0}^{12}x_l\cdot P_{l,0}\left(\sin\varphi\right). \tag{6.a}$$

The first experiment consists in to fit by Least Squares the expansion (6.a) to the NeQuick vTEC:

$$vTEC=\sum_{l=0}^{12}x_l\cdot P_{l,0}\left(\sin\varphi\right)=\int_{r_E+h_1}^{r_E+h_2}N\left(r,\varphi_L\right)\cdot dr+v. \tag{6.b}$$

The standard deviation of the residuals, σ_v<< ±0.1 TECu, confirms a good quality of fit.

The second experiment consists in to fit the expansion (6.a) to the NeQuick sTEC using the mapping function:

$$vTEC_L=\sum_{l=0}^{12}x_l\cdot P_{l,0}\left(\sin\varphi\right)=\cos z_L\left(h_L\right)\cdot\int_{r_E+h_1}^{r_E+h_2}N_{eNQ}\left(r,\varphi\right)\cdot\frac{dr}{\cos z}+v. \tag{6.c}$$

The standard deviation of the residuals increases (w.r.t. the previous experiment) to σ_v= ±5.3 TECu for h_L = 350 km, ±3.2 TECu for 400 km, ±3.7 TECu for 450 km, and ±5.7 TECu for 500 km.

The results of this experiment are summarized in Fig. 6.

The last experiment consists in to add the IFB, β, to the Eq. (6.c) and to estimate their values together with the expansion coefficients:

$$vTEC_L=\sum_{l=0}^{12}x_l\cdot P_{l,0}\left(\sin\varphi\right)+\beta(h_L)=\cos z_L\left(h_L\right)\cdot\int_{r_E+h_1}^{r_E+h_2}N_{eNQ}\left(r,\varphi\right)\cdot\frac{dr}{\cos z}+v. \tag{6.d}$$

The inclusion of additional unknowns reduces (w.r.t. the previous experiment) the standard deviations of the residuals: σ_v,= ±3.5 TECu for h_L = 350 km, ±2.6 TECu for 400 km, ±3.0 TECu for 450 km, and ±4.2 TECu for 500 km. Nevertheless, this fact does not imply any improvement in the estimation of the $vTEC_L$: in fact, $\left\langle\varepsilon\left(h_L\right)\right\rangle$ results significantly greater than in the previous experiment (Fig. 7).

Since the NeQuick $sTEC$ is not affected by DCB, any deviation from zero of the estimated $\beta(h_L)$ unknowns of Eq. (6.d) must be interpreted as an error, $\Delta\beta(h_L)$, due to the propagation of the mapping function errors to the estimated unknowns.

The systematic component of this error is characterized by the average of all the observed LOS (z_E from 0º to ±90º) from the 7 GNSS receivers:

$$\left\langle\Delta\beta(h_L)\right\rangle=\frac{1}{7}\sum_{\varphi_R=-40^\circ}^{\varphi_R=+20^\circ}\Delta\beta(h_L), \tag{7.a}$$

and the varying component is characterized by the average of the (absolute value) deviations:

$$\delta\Delta\beta\left(h_L\right)=\frac{1}{7}\sum_{\varphi_R=-40^\circ}^{\varphi_R=+20^\circ}\left|\Delta\beta\left(h_L\right)-\left\langle\Delta\beta\left(h_L\right)\right\rangle\right|. \tag{7.b}$$

Both estimates are shown in Fig. 8.

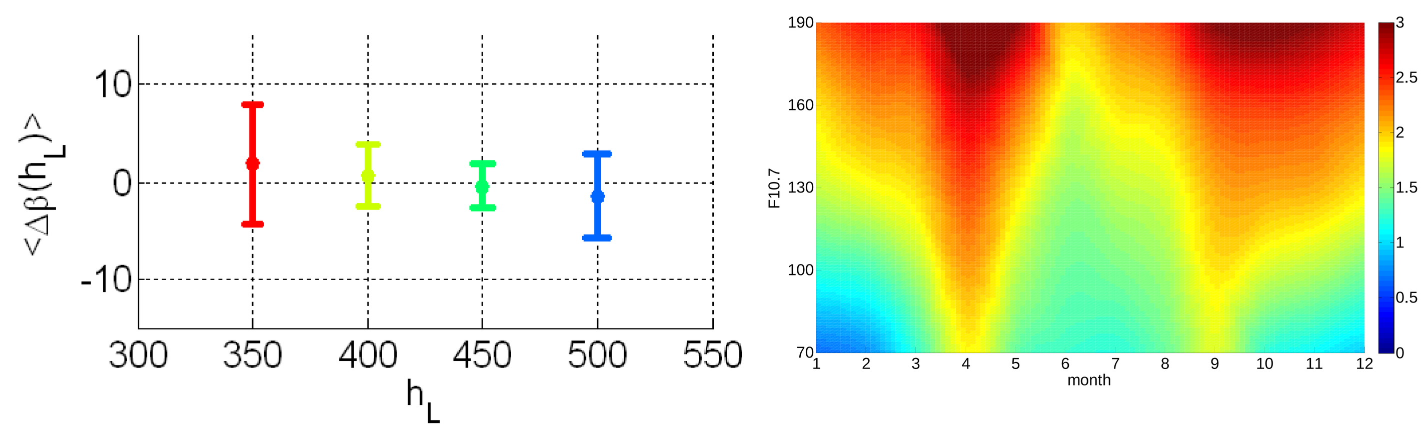

Fig. 8. Left: $\left\langle\Delta\beta(h_L)\right\rangle$ (points) and $\delta\Delta\beta(h_L)$ (bars) estimated from the Eq. (6.d) for h_L = 350, 400, 450 and 500 km, for high solar activity and March; right: variation with the solar activity and month of $\delta\Delta\beta\left(h_{L,0}\right)$ (TECu).

It should be noted that: i) the ionospheric layer height, $h_{L,0}$, that cancels the systematic bias in the vTEC estimation is, in general, different from the ionospheric layer height, $h'_{L,0}$, that cancels the systematic bias in the IFB estimation (Fig. 9, left); and ii) the simultaneous estimation of vTEC and DCB makes the systematic vTEC bias more sensitive (w.r.t. the estimation of vTEC without DCB) to ionospheric layer height changes (Fig. 9.right).

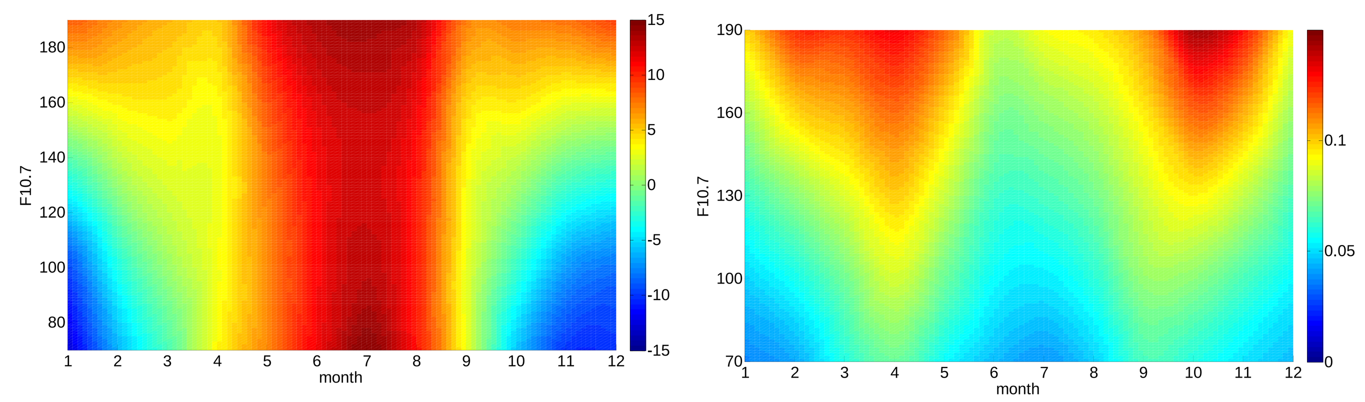

Fig. 9.Left: difference $\Delta h_{L,0}=h'_{L,0}-h_{L,0}$ (km) between the ionospheric layer heights, $h'_{L,0}$ that fulfils the condition $\left\langle\varepsilon\left\langle h'_{L,0}\right\rangle\right\rangle$= 0 and $h_{L,0}$ that fulfils the condition $\left\langle\varepsilon\left(h_{L,0}\right)\right\rangle$= 0; right: sensitivity (TECu/km) of the systematic bias $\left\langle\varepsilon\left(h_L\right)\right\rangle$ to the ionospheric layer height, h_L;

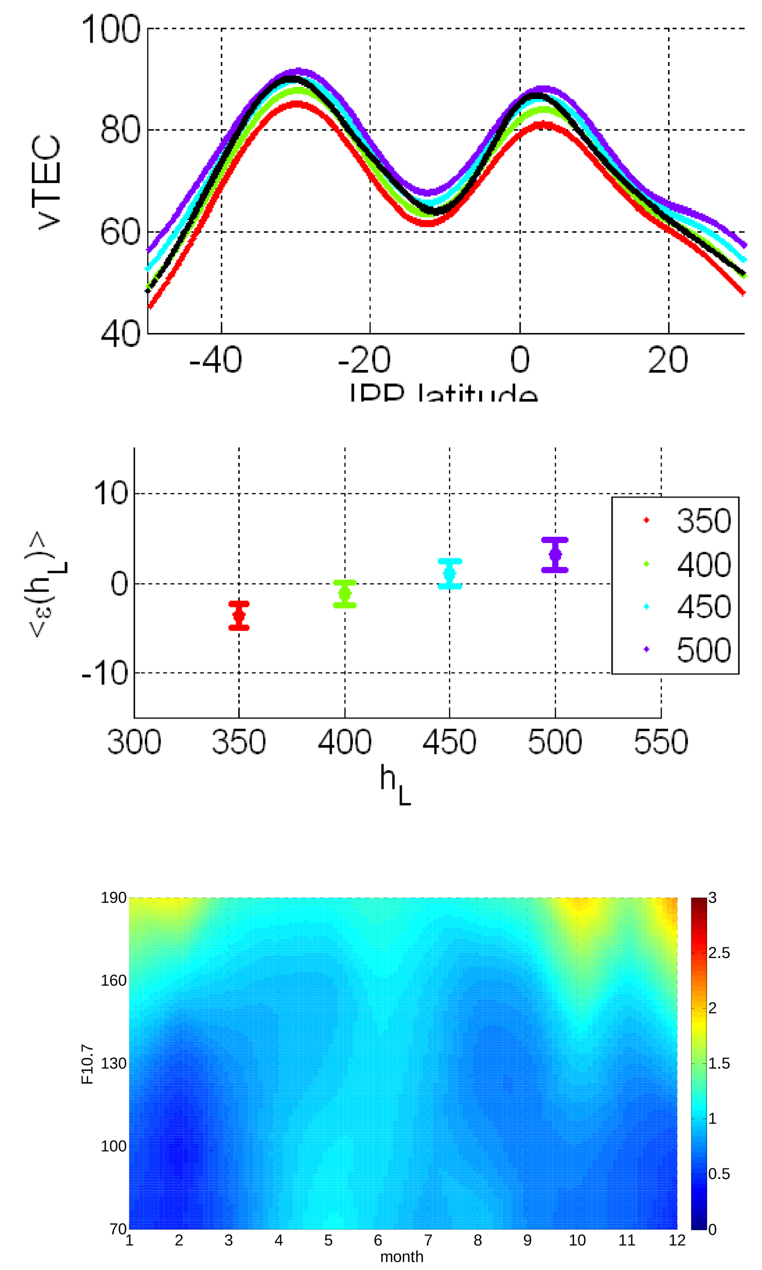

Fig. 6. Uppe figurer: $vTEC_L$ estimated from the Eq. (6.c) for h_L = 350, 400, 450 and 500 km (curves of different colours) and NeQuick vTEC (black curve) in TECu, for high solar activity and March; middle: variation with the height of the ionospheric layer, h_L (km), of $\left\langle\varepsilon\left(h_L\right)\right\rangle$ (points) and $\delta\varepsilon\left(h_L\right)$ (bars), in TECu, for high solar activity and March; bottom: variation with the solar activity and month of $\delta\varepsilon\left(h_{L,0}\right)$ in TECu.

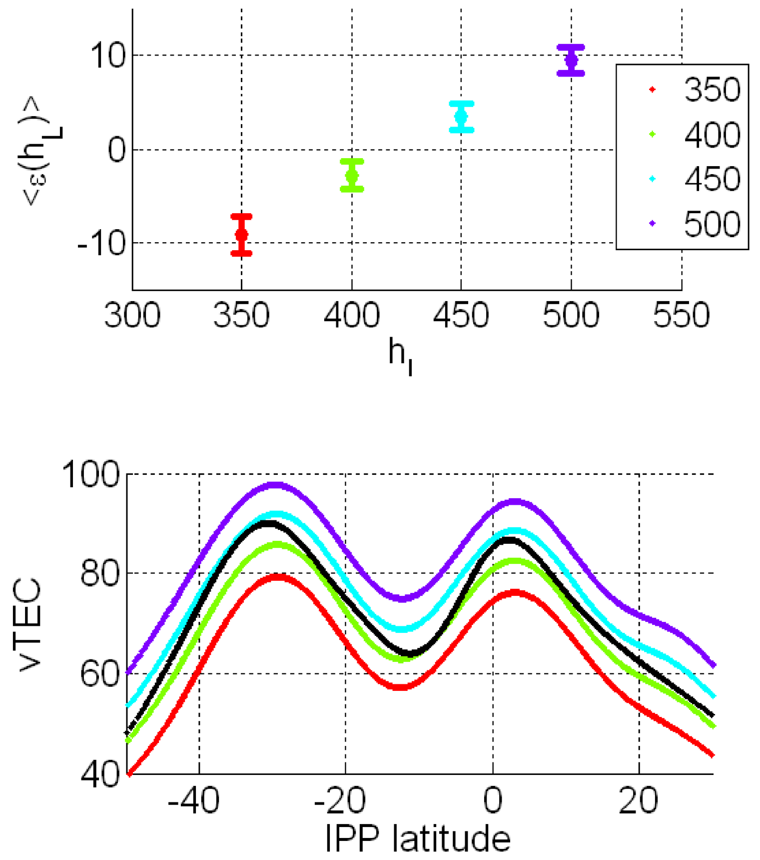

Fig. 7. Upper figure: $vTEC_L$ estimated from the Eq. (6.d) for h_L = 350, 400, 450 and 500 km (curves of different colours) and NeQuick vTEC (black curve) in TECu, for high solar activity and March; bottom: variation with the height of the ionospheric layer, h_L (km), of $\left\langle\varepsilon\left(h_L\right)\right\rangle$ (points) and $\delta\varepsilon\left(h_L\right)$ (bars), in TECu, for high solar activity and March.

6. Conclusions

The height of ionospheric layer is a key parameter of the thin layer ionospheric model. There is not any fixed height that reduces to zero the effects of the mapping function errors on the vTEC and DCB estimation. A fixed height for a given solar activity and month can be selected to reduce to zero the average of the vTEC bias for a given attitudinal range, but still remains a latitudinal varying residual error.

European Geophysical Union, 2010 General Assembly, Vienna, May 2-7, 2010.